JACS
JOURNAL OF THE AMERICAN CHEMICAL SOCIETY

ARTICLE

pubs.acs.org/JACS

Probing Multivalent Interactions in a Synthetic Host–Guest Complex by Dynamic Force Spectroscopy

Alberto Gomez-Casado, Henk H. Dam, M. Deniz Yilmaz, Daniel Florea, Pascal Jonkheijm,* and Jurriaan Huskens*

Molecular Nanofabrication Group, MESA+ Institute for Nanotechnology, University of Twente, P.O. Box 217, 7500AE Enschede, The Netherlands

Supporting Information

ABSTRACT: Multivalency is present in many biological and synthetic systems. Successful application of multivalency depends on a correct understanding of the thermodynamics and kinetics of this phenomenon. In this Article, we address the stability and strength of multivalent bonds with force spectroscopy techniques employing a synthetic adamantane/β-cyclodextrin model system. Comparing the experimental findings to theoretical predictions for the rupture force and the kinetic off-rate, we find that when the valency of the complex is increased from mono- to di- to trivalent, there is a transition from quasi-equilibrium, with a constant rupture force of 99 pN, to a kinetically dependent state, with loading-rate-dependent rupture forces from 140 to 184 pN (divalent) and 175 to 210 pN (trivalent). Additional binding geometries, parallel monovalent ruptures, single-bound divalent ruptures, and single- and double-bound trivalent ruptures are identified. The experimental kinetic off-rates of the multivalent complexes show that the stability of the complexes is significantly enhanced with the number of bonds, in agreement with the predictions of a noncooperative multivalent model.

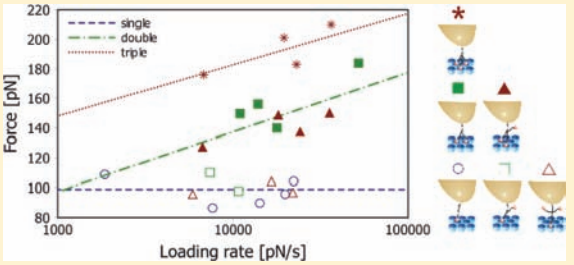

1. INTRODUCTION

Multivalency describes the interaction between multivalent receptors and ligands. It plays a pivotal role in biochemistry, governing many interactions between proteins and small molecules, between proteins or antibodies and cell membranes, between viruses and cells, etc.[1] At interfaces in particular, multivalency is poorly understood in a quantitative sense. Understanding of multivalent interactions at interfaces thus constitutes a way to better understand and control biological recognition events[2] and provides a tool to develop supramolecular nanomaterials.[3]

In principle, the usage of single-molecule techniques allows more detailed insight in the study of molecular interactions, in comparison with the traditional ensemble methods, such as calorimetry or NMR, on the macroscopic scale. Methods based on atomic force microscopy (AFM) and optical tweezers are more suited to register individual binding events and are employed to observe covalent and noncovalent bonds under controlled stress.[4] In particular, dynamic force spectroscopy (DFS) enables the determination of kinetic dissociation rate constants by analyzing the studied bond rupture at different loading rates, that is, how fast the bond is loaded with the external force.[5] Lifetimes of molecular complexes and even a detailed description of the energy landscape for some biological systems have been deduced using this technique.[6] Besides the study of complexes, the structure and unfolding pathways of proteins and mutant analogues such as titin[7] or the folding of the Parkinson-involved protein α-synuclein[8] have been examined as well using force spectroscopy. Moreover, modifications of this technique allow the construction of recognition maps on cellular membranes[9] or study the effect of mechanical stress on chemical reactions.[10]

To our knowledge, only three studies probing multivalency at the single molecule level by means of DFS have been reported before.[11] The complexes used for these studies were biological (concanavalinA–mannose,[11a] MUC1 antigen–antibody[11b]) and synthetic (C_{60}–porphyrin tweezers[11c]). Both studies using biomolecules concluded that the force of a multivalent bond scaled sublinearly with the number of bonds, whereas the C_{60}–porphyrin system yielded a divalent rupture force stronger than 2 times the monovalent rupture force. Presumably, this discrepancy could originate from the fact that the binding of C_{60} to porphyrin tweezers is likely to be not only multivalent but also strongly cooperative,[12] which would make the complex stronger than a purely multivalent attachment. On the other hand, the experiments using MUC1 antigen–antibody studied ruptures of parallel bonds, which have been predicted to break at reduced forces if the linkers connecting them are of different length.[13] In the case of the concanavalinA–mannose, conformational changes in the protein upon binding could change the affinity for successive

Received: February 21, 2011
Published: May 26, 2011

ACS Publications © 2011 American Chemical Society

Scheme 1. Compounds Used in This Study[a]

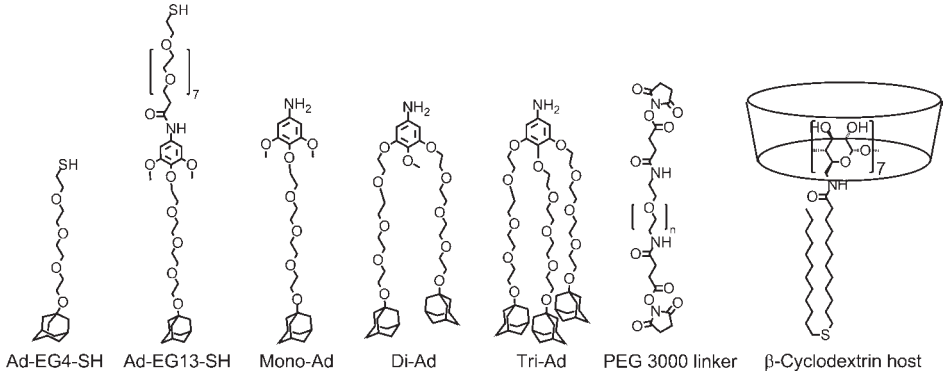

[a] Ad, adamantane; EG, ethyleneglycol; PEG, polyethyleneglycol.

Scheme 2. Tip Functionalization with Mono-Ad, Di-Ad, or Tri-Ad Using PEG3000 Linker[a]

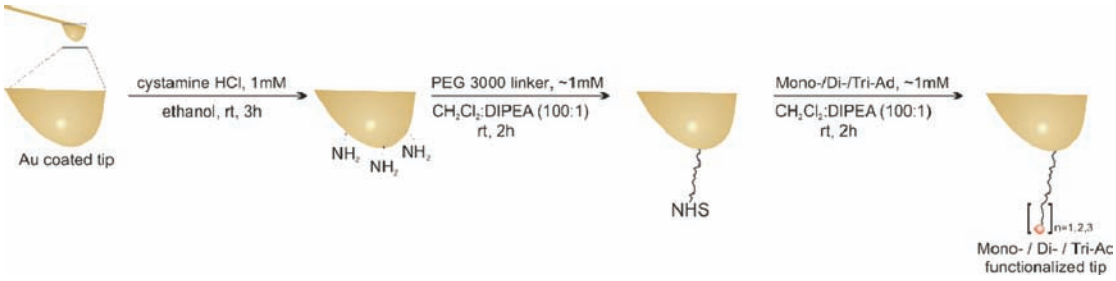

[a] Ad, adamantane; PEG, polyethyleneglycol; NHS, *N*-hydroxysuccinimide; DIPEA, *N*,*N*-diisopropylethyleneamine; rt, room temperature.

bindings. In this study, we use a synthetic host−guest system aiming to avoid the potential problems described above. The binding sites that are physically different molecules ensure that the affinities for the second and successive bonds are unaffected by the first, and the geometry of the multivalent guests is such that only one linker is pulled.

In our laboratory, we use the adamantane/β-cyclodextrin (βCD) supramolecular complex as a model system to study multivalency.[14] βCD is an oligosaccharide consisting of seven glucose units connected in a ring shape. The inner cavity of this ring is hydrophobic and can accommodate a wide variety of guest molecules.[15] This host−guest couple has been used by us for fabricating various nanostructures, and detailed SPR work in combination with thermodynamic models has provided insight in the multivalent characteristics of this interaction.[16] Previously, employing DFS we reported the rupture force between a series of monovalent guests bound to an AFM tip and surface-bound βCD. The notion of thermodynamic equilibrium allowed correlating quantitatively the measured pull-off force values with free binding energy of the complexes.[17]

Here, we provide a comprehensive thermodynamic and kinetic analysis of the binding of mono-, di-, and trivalent guests to self-assembled monolayers of βCD host. The interactions between single pairs of βCD and adamantane as well as between divalent and trivalent assemblies of these molecules were studied using DFS to study their binding forces and kinetic off-rates. A theoretical model for the multivalent assembly is used to compare the measured multivalent off-rates with the expected monovalent off-rate.

2. RESULTS AND DISCUSSION

2.1. Monovalent Guest. In a typical force spectroscopy (FS) experiment, several force curves are acquired using a functionalized AFM tip and/or substrate. Thus, βCD and adamantyl-functionalized molecules (Scheme 1) need to be immobilized in a convenient manner, one over the surface of the AFM tip and the other on a supporting substrate. We followed a well-known procedure to create a densely packed monolayer of βCD over a gold substrate, also known as the molecular printboard.[18] These printboards expose the hydrophobic cavities of βCD in a hexagonal lattice with a lattice constant of ca. 2 nm to the medium, effectively acting as a surface-bound multivalent receptor. The adamantyl (Ad) guests are readily attached to gold-coated AFM tips using thiol groups, either in a single-step procedure, when using short linkers, or successively connecting amine-reactive linkers and amino-functionalized guest moieties to a cysteamine monolayer (Scheme 2 and see the Experimental Section for a detailed description of the procedures for functionalizing the tip and substrate). For the study of multivalent guests, the spacers between the two Ad moieties must be chosen to be long enough to allow for multivalent complexation on the molecular printboard.[19] The functionalized tip and supporting substrate are installed in the AFM setup for the DFS experiment. A laser is employed to monitor the deflection of a soft cantilever connected to the tip. The distance between the base of this cantilever and the substrate is controlled by means of a piezoelectric crystal. Starting from a situation where the tip and substrate are not in contact, the distance between them is reduced (approach) until a positive deflection is detected. After a chosen delay during

which tip and surface remain in contact, the separation between substrate and cantilever base is progressively increased (retract). During this step, a negative deflection can be observed, which is related to an interaction between the tip and surface. When the energy accumulated in the bent cantilever is enough to break this interaction, the measured maximum deflection can be multiplied by the cantilever spring constant to give the unbinding force of the studied interaction. On a typical curve like the ones shown in Figure 1A, the retraction starts at the far left, and interactions with the surface are being broken until achieving the flat zero-force region, representing a relaxed cantilever.

Typically in FS studies the moieties of interest are not directly connected to the AFM tip surface; instead, a flexible linker is introduced between them to allow some translational and rotational freedom for complexation. In addition, this linker, if long enough, allows the rupture of the specific interaction pair to happen when the tip is several nanometers away from the surface and any nonspecific interactions between tip and surface have been already overcome. Furthermore, the characteristic non-linear elasticity of the linker can be used as an internal check of the measurements. A force curve measured using such linkers shows multiple ruptures. The first rupture event, a sudden change in the measured force, usually originates from unspecific short-range interactions between the tip and substrate. Subsequent events originate from the studied moieties being ruptured and should show a nonlinear region, characteristic of the particular linker in use, prior to the rupture. The slope of this curve immediately before the rupture is the instantaneous loading rate that is being applied to the bond (Figure 1C). Thus, the choice of a linker between an AFM tip and the guest molecules largely influenced the availability of rate data in our previous DFS studies,[17] where we used short linkers (alkyl chains of 7−18 carbons). Moreover, achieving and proving that the ruptures originate from a single host−guest pair is much more difficult with such sort linkers. Therefore, we decided to explore here the use of longer tethers between the monovalent guest and the tip surface. We chose three different water-soluble ethyleneglycol (EG) based linkers, that is, a short tetraethyleneglycol (Scheme 1A, EG4) linker, an EG13 (Scheme 1A) linker of intermediate length, and a long linker containing a polyethyleneglycol (PEG) chain of M_w 3000 g/mol (Scheme 1A, PEG 3000, approximately 68 ethyleneglycol units). In aqueous media,[20] we examined force−distance curves, selecting only those events that represent a polymer stretch region matching the expected single PEG chain behavior, which we used as an internal check of our measurements. A curve for each of these linkers is shown in Figure 1A, where it can be clearly seen how the separation between the first and final ruptures increases with the linker length. In addition, only in the case of the longest linker did we unequivocally observe nonlinear stretching behavior that could be reliably fitted to a worm-like chain (WLC) model[21] to obtain instantaneous loading rates, whereas in the case of the shorter linkers the transition in stiffness occurs too fast yielding too few data points for a reliable fitting procedure. With these results in hand, in the remainder of this study we employed the PEG 3000 linker (Figure 1B).

The collected force−distance curves, obtained from experiments where the monovalent adamantyl guest was linked to the tip via the PEG 3000 linker, were fitted to a WLC polymer model, where the contour length was the fitting parameter and the persistence length was fixed at a value of 3.5 Å, corresponding to one-half of the Kuhn length of 7 Å.[22] The fitted contour length

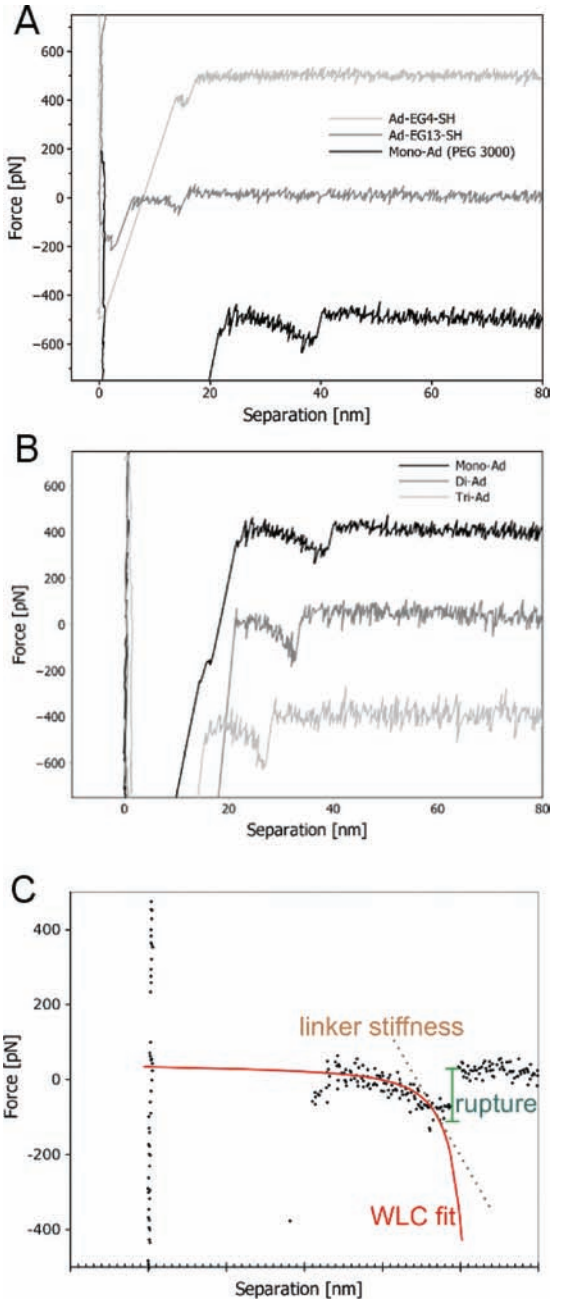

Figure 1. (A) Characteristic force−separation curves (offset in force axis for clarity) for monovalent adamantyl guests linked to the AFM tip by a short tetra ethylene glycol linker (EG4, top), linker with 13 EG units (EG13, middle), or a long linker of ca. 68 EG units (PEG3000, bottom). (B) Characteristic force−separation curves (offset in force axis for clarity) for mono-, di-, and trivalent adamantyl guests linked to the AFM tip by a long PEG3000 linker. (C) Example of a curve with highlighted rupture force and WLC (worm-like chain) fit to the data. The slope of this fit at the rupture point quantifies the stiffness of the polymer, and together with the retraction speed allows the calculation of the instantaneous loading rate.

(typically between 10 and 50 nm) was reasonably close to the expected value for a PEG chain of 3000 g/mol (average 25 nm), considering the polydispersity of the linker and the fact that we selected the last rupture event, which relates to the longest available linker on the tip. Next, the instantaneous loading rate

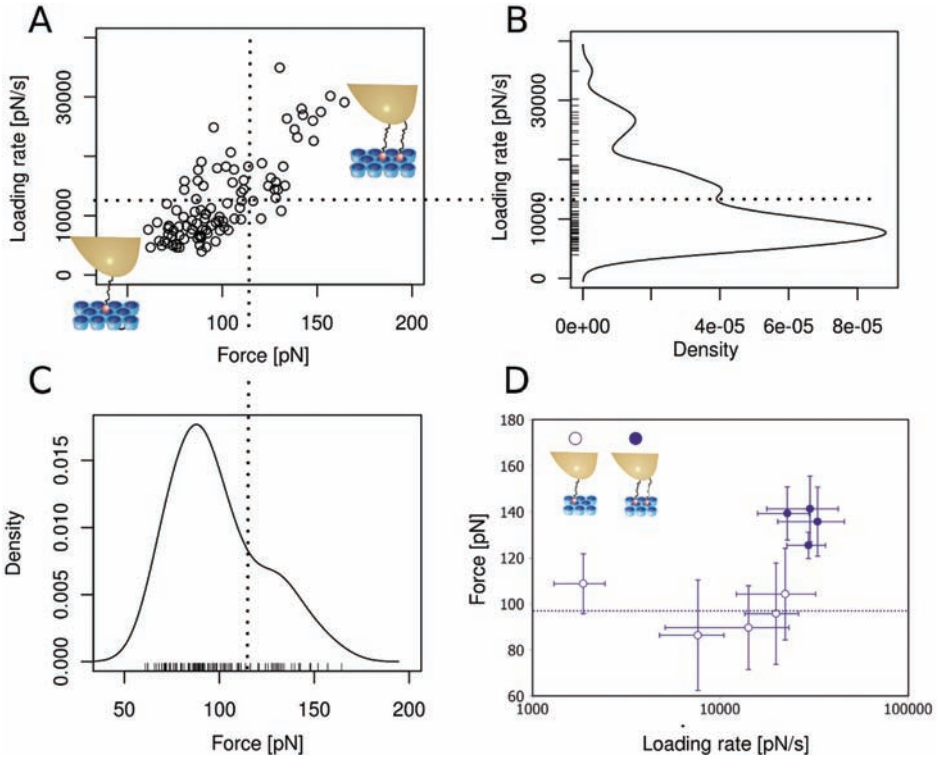

Figure 2. Analysis of DFS data of the monovalent guest (Mono-Ad) using PEG3000 linker. (A) Pairs of force and loading rate obtained from the collected curves and (B,C) kernel smoothened densities of probability constructed from them (the ticks indicate individual occurrences). Data corresponding to the main peaks of force and loading rate are assigned to monovalent binding, and the data corresponding to the high-force, high-rate tails of the distributions correspond to monovalent (parallel) binding. (D) Combined results from different retracting speeds; the dotted line is the averaged rupture force of a monovalent complex.

was calculated from the slope of the WLC fit at the rupture point (Figure 1C) to give pairs of force−loading rate values. For these forces and loading rates, an estimated density of probability was constructed. Such density graphs (Figures 2B,C) show what forces and loading rates were observed for each set of pulling conditions. On some of the force probability densities a long high-force tail or even a well-defined secondary peak was found (Figure 2C). Crossing these data with the loading rate data, where also a long tail was present, we found that data points can be grouped into two quadrants (Figure 2A). One group consists of low force/low rate data points, which relate to monovalent force, and another group consists of high force/high rate data points, which we tentatively attribute to the parallel rupture of two monovalent host−guest pairs. In this latter case, the rupture force value has been predicted to vary with the difference in length of the chains that link the two guests, being lower when the two pairs are linked by chains of different lengths as compared to the situation when both chains are of identical length.[13]

To perform further analysis on the monovalent data, we made use of a theory developed by Evans et al.[5] based on previous work by Bell,[23] which predicts linear scaling of the rupture force f to the logarithm of the loading rate r, where k_B is the Boltzmann constant, T is the temperature, Δx is the width of the energy barrier, and k_{off} is the intrinsic dissociation rate (the dissociation rate constant when the bond is not loaded by an external force).

$$f = \frac{k_B T}{\Delta x} \ln\left(\frac{r \Delta x}{k_{off} k_B T}\right) \quad (1)$$

When the data of the monovalent guest were plotted in this way (open symbols in Figure 2D), a zero slope was observed in the explored loading rate range, indicating that the complex can be considered in thermodynamic equilibrium for our experimental conditions, in agreement with our previous studies on monovalent guests[17,24] and other systems.[25] In addition, the most apparent rupture force in the case of the monovalent adamantane guest, 97 ± 19 pN, closely matches our previous results obtained for short tethers (102 ± 15 pN).[17] This loading rate-independent behavior can be explained by the fact that the binding and unbinding rate constants for the cyclodextrin−adamantane system (k_{on} is diffusion limited, on the order of 10^8 M^{-1} s^{-1},[26] and k_{off} estimated to be 2×10^3 s^{-1} for a measured equilibrium constant,[16a] $K_{eq} = 4.6 \times 10^4$ M^{-1}) represent a very rapid equilibration as compared to the time scale of the AFM measurements. The monovalent guest probed under these conditions can be considered at thermodynamic equilibrium, and thus no kinetic effects such as the unbinding force dependence on loading rate are expected to show up in the measurements. This aspect could be confirmed by implementing a model[27] that predicts the transition from equilibrium to a dynamic regime. The estimated potential of the adamantane−cyclodextrin interaction was introduced in such model (see the Supporting Information), obtaining an equilibrium rupture force of 90 pN and an unforced off-rate of 2×10^3 s^{-1}, which are very close to the values presented above. The loading rate required to observe the characteristic logarithmic increase of rupture forces is estimated as 10^7−10^8 pN/s, well beyond the range of AFM-based DFS. Loading rate dependence could not

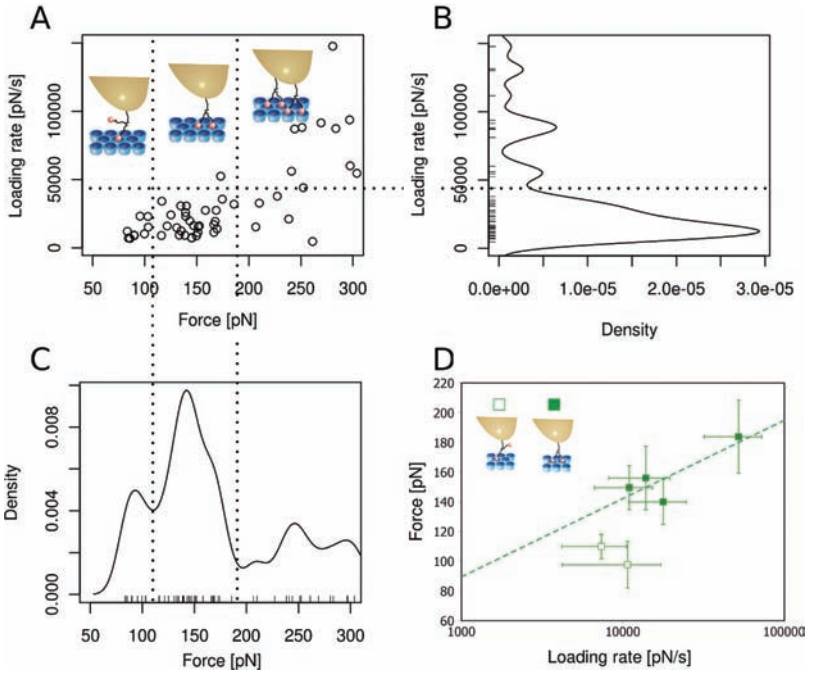

Figure 3. Analysis of DFS data of the divalent guest (Di-Ad) using PEG3000 linker. (A) Pairs of force and loading rate obtained from the collected curves. (B,C) Kernel smoothened densities of probability constructed from them (the ticks indicate individual occurrences). The main peak on the force distribution is assigned to divalent force (divalent-double, filled symbols), and the secondary peak at lower force (when present) is assigned to pull-offs were only a single adamantane was bound in the instant of rupture (divalent-single, open symbols). Data corresponding to the high-force, high-rate tails originate from several possible situations were more than one divalent host−guest complex was ruptured. Notice that because only one linker is involved in divalent-single and divalent-double ruptures, both fall in the same band of loading rates. (D) Combined results from different retracting speeds; the dashed line is a logarithmic fit as a guide to the eye.

be assessed for the parallel monovalent unbinding events (filled symbols in Figure 2D), because all ruptures occurred at similar loading rates.

2.2. Divalent Guest. Following the same attachment procedure using the PEG 3000 linker to the AFM tip, we collected and analyzed force−distance curves for the divalent guest (Figure 3A). In strong contrast to the monovalent guest, the most probable rupture force was found to be dependent on the loading rate, ranging from 140 ± 15 pN (probe retraction speed 260 nm s^{-1}) to 184 ± 25 pN (probe retraction speed 1160 nm s^{-1}). The rupture forces for divalent guests were in all cases smaller than twice the rupture force for monovalent guests, in agreement with theoretical predictions[28] and experimental studies.[11a,b,13] However, when crossing the distributions of rupture force and loading rate (Figure 3), we clearly distinguish three regions. The most probable loading rate comprised two characteristic rupture force peaks. The lower of these two peaks indicates a rupture force matching the values of the previously determined monovalent unbinding force and can be interpreted as events where only one of the adamantyl moieties was bound at the moment of rupture (named as divalent-single in the rest of this Article). The higher and most probable force corresponds to divalent ruptures (divalent-double). Finally, a third region consists of high-force, high-loading rate events, which we attribute to parallel unbinding of two (or more) divalent guests. Because these data can originate from several binding situations (double+double, single+single, and single+double bound for two parallel divalent guests), further analysis was not performed.

One important aspect revealed by these experiments is the difference between multivalent and parallel arrangements. It has been previously reported that the difference in length between two linkers in a parallel rupture will lead to lower rupture forces.[13] In the case of probing two host−guest complexes, the maximum rupture force will be measured when the linkers are loaded under identical conditions at the moment of the rupture. This implies that both chains are of the same length, which is not likely when using long polymeric linkers, and their attachments points are such that both distances to the surface are equal. The geometry of our divalent guest is the optimal approach to achieve simultaneous and equal loading, because the two host−guest pairs are connected by a single linker and branch out only at the very end. The measured higher rupture forces in the case of the divalent guest (approximately 170 pN at 30 nN/s) when compared to parallel monovalent guests (approximately 140 pN at 30 nN/s) confirm the prediction that linking the guest moieties through a single tether is the optimal approach to measure multivalent interactions.

When more than one weak moiety is attached in a multivalent fashion, the dissociation rate constant is expected to decrease several orders of magnitude,[16b,29] opening the possibility to probe the complex in an out-of-equilibrium regime. This is confirmed here by measuring rupture forces for divalent-double cyclodextrin−adamantane complexes, which presented a defined loading rate dependency.

2.3. Trivalent Guest. Experiments using the trivalent guest were performed in the same manner as described above. The density of probability of measured rupture forces showed multiple peaks over a large range of forces (see the Supporting Information). We discussed above that high force peaks originate from parallel ruptures. In the case of two trivalent guests rupturing

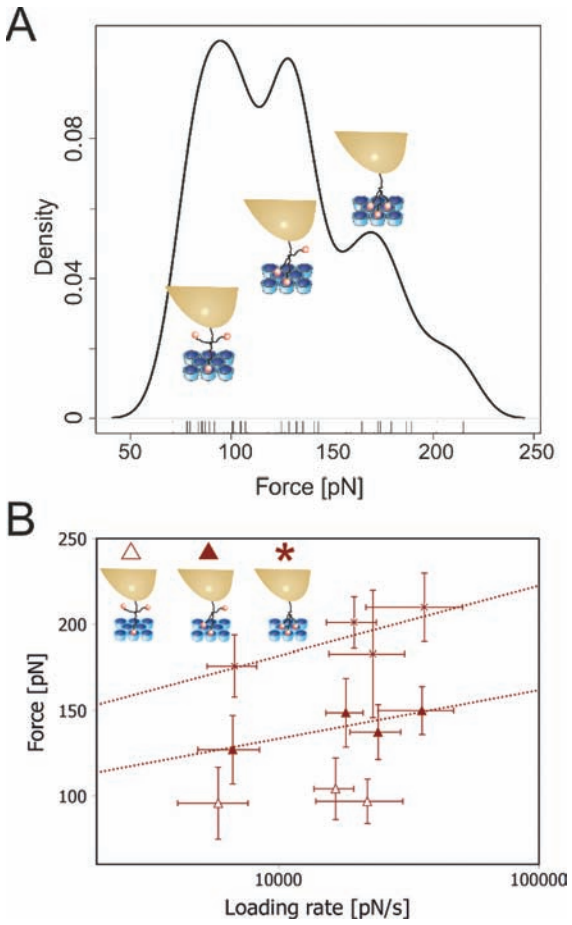

Figure 4. Results from the analysis of DFS data of trivalent guest (Tri-Ad) using PEG3000 linker. (A) Kernel smoothened density of probability of rupture forces corresponding to the main peak of the loading rate distribution (the ticks indicate individual occurrences). The three different peaks are assigned (from lower to higher force) to ruptures of trivalent-single (open symbols), -double (filled symbols), and -triple (stars) bound guest. (B) Combined results from different retracting speeds; the dotted lines are logarithmic fits for the second and third peaks as a guide to the eye.

simultaneously, the forces cannot only be relatively high (triple+triple, triple+double, double+double) but also appear in a range of forces very near divalent characteristic forces (single+single) and between divalent and trivalent forces (single+double). We have shown that parallel ruptures are characterized by higher instantaneous loading rates as compared to ruptures where only a single linker is being stretched. This fact enables us to filter out the FS data collected using trivalent guests by selecting only the data corresponding to the main loading rate peak to discard these parallel ruptures (see Figure S5 in the Supporting Information). After such a procedure, the rupture forces of the remaining events were used to construct density graphs where three distinct force peaks could be resolved (Figure 4). A straightforward explanation for the meaning of these three characteristic forces is to consider that the lower, middle, and higher force peaks originate from ruptures where one (trivalent-single), two (trivalent-double), or three (trivalent-triple) adamantyl moieties, respectively, were bound. Moreover, the rupture forces determined by the lower force peak compare well to the unbinding force of a monovalent complex of ca. 100 pN, while the rupture forces determined by

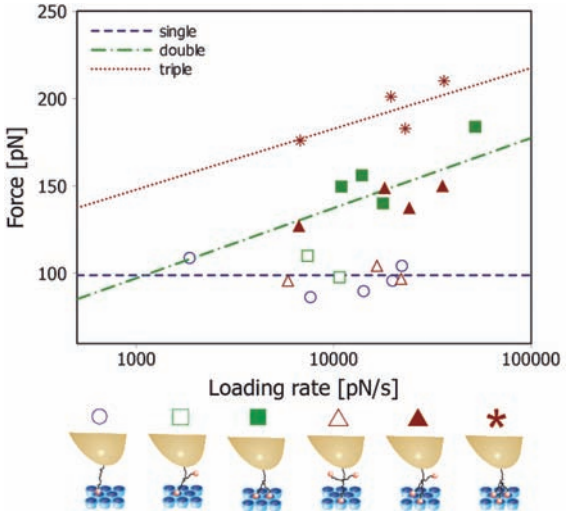

Figure 5. Comparison of AFM-DFS data of mono-, di-, and tri-adamantyl guests. Different attachment geometries are assigned, single bound mono-, di-, and trivalent (open symbols), double bound di- and trivalent (filled symbols), and triple bound trivalent (stars). The lines are least-squares fits to the Evans model for the double and triple bound data, and the average rupture force for the single bound data.

Table 1. Parameters Obtained by Fitting FS Data to Bell−Evans Model[a]

bond valency	monovalent (estimated)	double	triple
Δx (nm)	0.2−0.3	0.24 ± 0.09	0.27 ± 0.10
k_{off} (s^{-1})	2000[31]	0.2 (0.01−3.5)	0.004 (0.0003−0.05)

[a] For k_{off}, a confidence interval is given in parentheses.

the middle peak compare well to the values and trend of the divalent-double ruptures (Figure 5), which confirms our interpretation of the force density graphs for the trivalent guest. The rupture force of a fully bound trivalent complex showed a stronger dependence on the loading rate, with values ranging from 175 ± 18 pN (probe retraction speed 581 nm s^{-1}) to 210 ± 20 pN (probe retraction speed 2620 nm s^{-1}), when compared to the measured forces for the divalent complex at similar loading rates.

2.4. Kinetic Analysis. The monovalent adamantyl−βCD system appears to be at equilibrium under the accessible conditions for loading rate and acquisition bandwidth. Therefore, the Bell−Evans model (eq 1), developed for dissociations occurring out-of-equilibrium, can not be applied to our data to obtain a value for k_{off} for the monovalent system based on force spectroscopy. However, the experimental data from divalent and trivalent guests show a pronounced loading rate dependence of the rupture forces, making them suitable for a fit. The values of Δx and k_{off} for ruptures of double (from divalent-double and trivalent-double data) and triple (from trivalent-triple data) attachments are presented in Table 1. From these data, an increased stability of the complex is clearly observed upon increasing the valency, with lifetimes extended 100- to 10 000-fold per each extra bond. Such enhanced stability is a general feature of multivalent complexes and responsible for multivalent strategies serving as design criteria for novel (macro)molecules for biomedical applications.[30]

Scheme 3. Diagram of Multivalent Equilibrium and Stepwise Kinetics

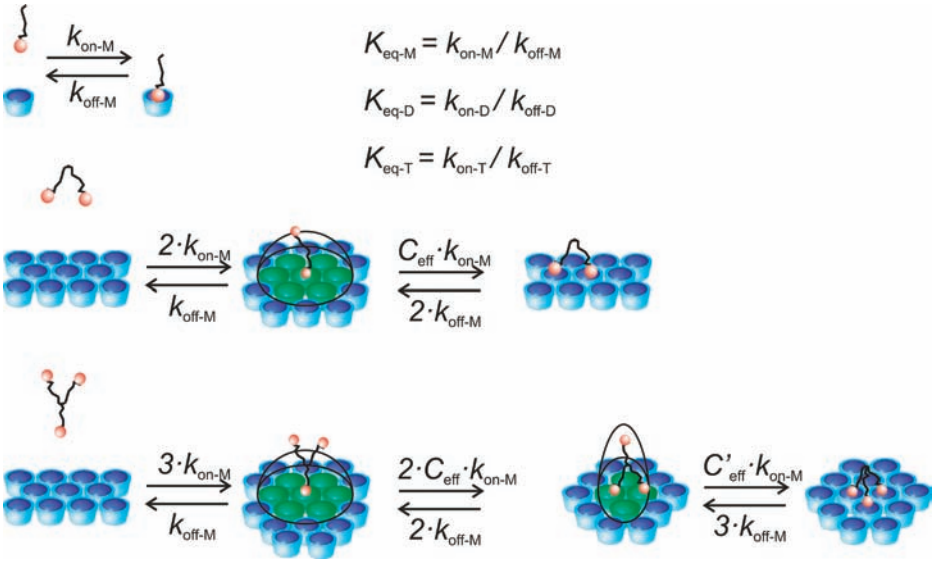

2.5. Comparison of DFS Results with Theoretical Model for Multivalent Dissociation. A model predicting the thermodynamics and kinetics of multivalent assemblies has been proposed[16b] and validated for divalent host−guest systems like the one in our study.[16a] The multivalent binding/unbinding process can be described in a stepwise manner as depicted in Scheme 3; an intermolecular binding is followed by successive intramolecular steps where the intrinsic binding affinity is unchanged. This model explains the enhanced binding affinity by a high local effective concentration (C_{eff}) of the host that is available for the divalent guest molecule when it is bound through only one of its guest moieties (divalent-single). Thus, no cooperativity in the sense of an increase of intrinsic binding affinity from the first to the second binding is assumed.[12] The expected equilibrium constant for a multivalent complex can be related to the corresponding monovalent constant according to this scheme. For clarity, the trivalent rates and equilibrium constants are here given the subscript "T" and their monovalent and divalent counterparts the subscripts "M" and "D", respectively. In the case of a divalent complex, we have:

$$K_{eq\text{-}D} = \frac{2k_{on\text{-}M}\cdot k_{on\text{-}M}C_{eff}}{k_{off\text{-}M}\cdot 2k_{off\text{-}M}} = K_{eq\text{-}M}^2 C_{eff} \quad (2)$$

Because the association rate in this system is diffusion limited, we propose $k_{on} = 10^8\ M^{-1}\ s^{-1}$ in the case of the monovalent adamantyl/βCD system. In the case of the divalent guest, a statistical factor 2 is introduced.

$$k_{on\text{-}D} = 2k_{on\text{-}M} \quad (3)$$

$$K_{eq\text{-}D} = \frac{k_{on\text{-}D}}{k_{off\text{-}D}} \quad (4)$$

We can combine eqs 2−4 to obtain a relationship between the monovalent and divalent off-rate constants:

$$\frac{k_{off\text{-}M}}{k_{off\text{-}D}} = \frac{1}{2}K_{eq\text{-}M}C_{eff} \quad (5)$$

The values for $K_{eq\text{-}M}$ ($4.6 \times 10^4\ M^{-1}$) and C_{eff} (0.2 M) were determined in previous studies[16a] using the same βCD and adamantyl host−guest system. In particular, the value of C_{eff} indicates that the second guest moiety is only able to complex with the (approximately 6) host cavities directly near the already occupied cavity. Thus, we can estimate the value for the unforced off-rate of a monovalent guest:

$$k_{off\text{-}M(estimated)} = \frac{k_{on\text{-}M}}{K_{eq\text{-}M}} = 2 \times 10^3\ s^{-1}$$

Substituting this value in eq 5 for a model-based estimation of the unforced off-rate of a divalent guest gives:

$$k_{off\text{-}D(estimated)} = \frac{2\cdot k_{off\text{-}M(estimated)}}{K_{eq\text{-}M}C_{eff}} = 0.47\ s^{-1}$$

This estimated value for the divalent off-rate is remarkably close to the value ($0.2\ s^{-1}$) found after fitting the Evans model to our DFS data. The strong agreement between these two values for $k_{off\text{-}D}$ confirms that the enhanced unbinding force for a double-bound guest can be fully attributed to multivalency effects, which was our main aim when designing the structure of the guest molecules.

A similar derivation can be done for the trivalent guest; in this case, we introduce in the last step (Scheme 3) the parameter $C'_{eff} = C_{eff}/3$, because there are only two accessible cavities for the third guest moiety once a double bond has been established. Taking this into account, we estimated the off-rate of a trivalent guest to be:

$$k_{off\text{-}T(estimated)} = \frac{9\cdot k_{off\text{-}M(estimated)}}{(K_{eq\text{-}M}C_{eff})^2} = 2 \times 10^{-4}\ s^{-1}$$

This theoretical value and the experimentally observed $k_{off\text{-}T}$ ($4 \times 10^{-3}\ s^{-1}$) agree remarkably, and we tentatively ascribe the small discrepancy to the conformational difference of the ethyleneglycol linkers in a fully bound trivalent and a fully bound divalent complex (see the Supporting Information). The introduction of an additional bond significantly stabilizes the trivalent

dx.doi.org/10.1021/ja2016125 |J. Am. Chem. Soc. 2011, 133, 10849–10857

complex over 100-fold as compared to the fully bound divalent complex, confirming the characteristical binding of a multivalent ligand onto independent binding sites.

3. CONCLUSIONS

We measured rupture forces of mono-, di-, and trivalent complexes of the β-cyclodextrin−adamantyl host−guest pair. The monovalent complex was probed at equilibrium, while the divalent and trivalent showed a significant loading rate dependency. The rupture forces of the fully bound divalent and trivalent complexes were found to be less than twice and thrice, respectively, that of the monovalent complex. However, the transition between the equilibrium regime (monovalent) and the kinetic regime (divalent and trivalent) so far prevents a more meaningful comparison of these rupture forces to further confirm a particular scaling law.

Additionally, we could identify events where two parallel monovalent complexes were dissociating. Although the two single binding moieties are chemically identical to the case of a fully bound divalent complex, differences of length or load between the two parallel tethers lowered the measured rupture force with respect to the rupture force of a divalent complex. The geometry of the multivalent guests employed in this study, with only one tether pulling at the complex, allowed us to achieve a situation equivalent to two or three equal parallel tethers, an optimal condition for obtaining more reliable results when studying multivalent interactions. Ruptures of lower force, matching the forces of monovalent or divalent ruptures, were observed in some of the experiments using multivalent guests. This suggests that at the moment of rupturing, the multivalent guests were partially bound to the CD printboard.

Finally, we found our initial assumption for our system, noncooperative multivalency, confirmed by the kinetic off-rate values obtained from the analysis of the DFS experiments performed using multivalent adamantly guests.

4. EXPERIMENTAL SECTION

Materials. All solvents were purchased from commercial sources and used as received. Cystamine hydrochloride, PEG 3000 (NHS-terminated homobifunctional PEG, M_W 3000), and 2-mercaptoethanol were purchased from Sigma-Aldrich. βCD adsorbate was synthesized as described previously.[18] Detailed synthesis of compounds shown in Scheme 1 can be found in the Supporting Information.

Cyclodextrin Monolayer. All glassware was cleaned to remove organic contamination by using piranha solution (3:1 mixture of sulfuric acid and hydrogen peroxide) and thoroughly rinsed with MQ water and ethanol.

Gold-coated (200 nm thickness) glass squares were purchased from Arrandee (Arrandee, Germany). After being rinsed with chloroform, they were annealed under a high purity hydrogen flame for about 5 min and allowed to cool. CD adsorbate (1−2 mg) was dissolved in a 3:2 solution of chloroform and ethanol (total volume 50 mL). The gold substrates were immersed in fresh piranha solution for 10−20 s to remove any organic contamination, rinsed with MQ water and ethanol, and immediately put into the CD solution. The samples were kept in this solution overnight at 60 °C, rinsed sequentially with dichloromethane, ethanol, and MQ water to remove any excess of adsorbed material, and used immediately in the force spectroscopy experiments.

Functionalization of AFM Tips. Gold-coated V-shaped AFM cantilevers with pyramidal tips (Veeco, Digital Instruments, U.S.) were cleaned in piranha solution for 10 s, then carefully rinsed with MQ water and ethanol. In the case of Ad-EG4-SH functionalization, the cantilevers were immersed in an ethanol solution of 0.5% Ad-EG4-SH and 99.5% 2-mercaptoethanol (1 mM total thiol concentration) overnight. For the Ad-EG13-SH functionalization, the cantilevers were immersed in an ethanol solution of 25% Ad-EG13-SH and 75% 2-mercaptoethanol (1 mM total thiol concentration) overnight. Finally, the cantilevers were rinsed with ethanol and blown dry in a stream of nitrogen. For the PEG 3000 functionalization, the cantilevers were cleaned as described before and immersed in an ethanol solution of cystamine hydrochloride (1 mM) for 3 h. After being rinsed with ethanol and dichloromethane, the amine terminated cantilevers were incubated for 2 h in a 100:1 dichloromethane/DIPEA solution with PEG 3000 linker (NHS-PEG-NHS, 5 mg/mL, ∼1 mM) and rinsed with dichloromethane. Finally, they were immersed for 2 h in a solution of amino terminated mono-, di-, or tri-adamantane guest (1 mM) in 100:1 dichloromethane/DIPEA, rinsed with dichloromethane, and blown dry in a stream of nitrogen.

AFM Force Spectroscopy Measurements. All force measurements were performed with a commercial Multimode Picoforce SPM (Veeco, Digital Instruments, U.S.) using a liquid cell (Veeco) and stock PBS buffer (B. Braun Melsungen AG, Germany). The spring constants of the cantilevers were calibrated using the built-in thermal tune software. Force−distance curves were acquired by approaching and retracting the tip at speeds ranging from 10 to 10^3 nm/s. The tip was laterally displaced over the substrate between each approach−retraction cycle, covering 1 μm^2, and the maximum force applied to the surface was kept under 500 pN. Two different cantilevers were used for each guest. We could obtain up to 5000 curves per cantilever, limited by the appearance of high adhesion between the tip and surface and a large decrease in the chance of observing polymer stretching. This we attribute to deterioration of the monolayers due to the repeated contact or adsorption of contamination on the tip.

Data Analysis. We selected relevant force curves using our own plug-in script developed for Hooke.[32] Each curve was examined for sudden changes in force (rupture events), and then the data prior to the last rupture (the unbinding event happening farthest away from the surface) were fitted using a WLC model with fixed persistence length 3.5 Å. Rupture events were rejected or kept for further analysis based on the quality of the fit, which was assessed visually and numerically by comparing the averaged force difference from each data point to the corresponding fitted force $d_{D\text{-}F}$ with the standard deviation of the measured force in the noncontact area σ_{NC} (see more details in the Supporting Information). If the ratio of these two parameters is close to 1, the difference between the fit and data can be explained by thermal noise. Pairs of rupture force and instantaneous loading rate were obtained from the valid events, and an estimation of the rupture force and loading rate probability densities was obtained with the help of the statistical package R,[33] by using kernel density estimation with Epanechnikov kernels and a fixed bandwidth of 10 pN in the case of force or an automatically selected bandwidth (Sheather and Jones algorithm)[34] in the case of loading rate and contour length.

■ ASSOCIATED CONTENT

Supporting Information. Synthesis of compounds, details of the force−distance curve filtering procedure, density of probability graphs of force, loading rate, and contour length for mono-, di-, and trivalent guests, comparison of the monovalent equilibrium rupture force with a theoretical model, and additional details about the stability of the fully bound trivalent guest. This material is available free of charge via the Internet at http://pubs.acs.org.

■ AUTHOR INFORMATION

Corresponding Author
p.jonkheijm@utwente.nl; j.huskens@utwente.nl

■ ACKNOWLEDGMENT

We thank the Dutch nanotechnology network NanoNed (Project No. TPC 6939) for financial support. P.J. thanks the Dutch Science Council of the Chemical Sciences for a VENI grant (700.57.401).

■ REFERENCES

(1) (a) Ehrlich, P. H. *J. Theor. Biol.* **1979**, *81*, 123–7. (b) Thobhani, S.; Ember, B.; Siriwardena, A.; Boons, G. J. *J. Am. Chem. Soc.* **2003**, *125*, 7154–5. (c) Scobie, H. M.; Young, J. A. *Curr. Opin. Microbiol.* **2005**, *8*, 106–12.

(2) (a) Kiessling, L. L.; Gestwicki, J. E.; Strong, L. E. *Angew. Chem., Int. Ed.* **2006**, *45*, 2348–68. (b) Martos, V.; Castreno, P.; Valero, J.; de Mendoza, J. *Curr. Opin. Chem. Biol.* **2008**, *12*, 698–706. (c) Sriram, S. M.; Banerjee, R.; Kane, R. S.; Kwon, Y. T. *Chem. Biol.* **2009**, *16*, 121–31.

(3) (a) Badjic, J. D.; Nelson, A.; Cantrill, S. J.; Turnbull, W. B.; Stoddart, J. F. *Acc. Chem. Res.* **2005**, *38*, 723–32. (b) Mulder, A.; Huskens, J.; Reinhoudt, D. N. *Org. Biomol. Chem.* **2004**, *2*, 3409–24.

(4) (a) Bizzarri, A. R.; Cannistraro, S. *Chem. Soc. Rev.* **2010**, *39*, 734–749. (b) Neuman, K. C.; Nagy, A. *Nat. Methods* **2008**, *5*, 491–505.

(5) Evans, E.; Ritchie, K. *Biophys. J.* **1997**, *72*, 1541–55.

(6) (a) Merkel, R.; Nassoy, P.; Leung, A.; Ritchie, K.; Evans, E. *Nature* **1999**, *397*, 50–3. (b) Hummer, G.; Szabo, A. *Acc. Chem. Res.* **2005**, *38*, 504–13. (c) Harris, N. C.; Song, Y.; Kiang, C. H. *Phys. Rev. Lett.* **2007**, *99*, 068101. (d) Odorico, M.; Teulon, J. M.; Bessou, T.; Vidaud, C.; Bellanger, L.; Chen, S. W.; Quemeneur, E.; Parot, P.; Pellequer, J. L. *Biophys. J.* **2007**, *93*, 645–654.

(7) (a) Marszalek, P. E.; Lu, H.; Li, H.; Carrion-Vazquez, M.; Oberhauser, A. F.; Schulten, K.; Fernandez, J. M. *Nature* **1999**, *402*, 100–3. (b) Rief, M.; Gautel, M.; Oesterhelt, F.; Fernandez, J. M.; Gaub, H. E. *Science* **1997**, *276*, 1109–12.

(8) (a) Yu, J.; Malkova, S.; Lyubchenko, Y. L. *J. Mol. Biol.* **2008**, *384*, 992–1001. (b) Sandal, M.; Valle, F.; Tessari, I.; Mammi, S.; Bergantino, E.; Musiani, F.; Brucale, M.; Bubacco, L.; Samori, B. *PLoS Biol.* **2008**, *6*, e6.

(9) Duman, M.; Pfleger, M.; Zhu, R.; Rankl, C.; Chtcheglova, L. A.; Neundlinger, I.; Bozna, B. L.; Mayer, B.; Salio, M.; Shepherd, D.; Polzella, P.; Moertelmaier, M.; Kada, G.; Ebner, A.; Dieudonne, M.; Schutz, G. J.; Cerundolo, V.; Kienberger, F.; Hinterdorfer, P. *Nanotechnology* **2010**, *21*, 115504.

(10) Garcia-Manyes, S.; Liang, J.; Szoszkiewicz, R.; Kuo, T.-L.; Fernández, J. M. *Nat. Chem.* **2009**, *1*, 236–242.

(11) (a) Ratto, T. V.; Rudd, R. E.; Langry, K. C.; Balhorn, R. L.; McElfresh, M. W. *Langmuir* **2006**, *22*, 1749–57. (b) Sulchek, T.; Friddle, R. W.; Noy, A. *Biophys. J.* **2006**, *90*, 4686–91. (c) Zhang, Y.; Yu, Y.; Jiang, Z.; Xu, H.; Wang, Z.; Zhang, X.; Oda, M.; Ishizuka, T.; Jiang, D.; Chi, L.; Fuchs, H. *Langmuir* **2009**, *25*, 6627–32.

(12) Ercolani, G. *J. Am. Chem. Soc.* **2003**, *125*, 16097–103.

(13) Guo, S.; Ray, C.; Kirkpatrick, A.; Lad, N.; Akhremitchev, B. B. *Biophys. J.* **2008**, *95*, 3964–3976.

(14) Ludden, M. J. W.; Reinhoudt, D. N.; Huskens, J. *Chem. Soc. Rev.* **2006**, *35*, 1122–34.

(15) Szejtli, J. *Chem. Rev.* **1998**, *98*, 1743–1754.

(16) (a) Mulder, A.; Auletta, T.; Sartori, A.; Del Ciotto, S.; Casnati, A.; Ungaro, R.; Huskens, J.; Reinhoudt, D. N. *J. Am. Chem. Soc.* **2004**, *126*, 6627–36. (b) Huskens, J.; Mulder, A.; Auletta, T.; Nijhuis, C. A.; Ludden, M. J.; Reinhoudt, D. N. *J. Am. Chem. Soc.* **2004**, *126*, 6784–97.

(17) Auletta, T.; de Jong, M. R.; Mulder, A.; van Veggel, F. C.; Huskens, J.; Reinhoudt, D. N.; Zou, S.; Zapotoczny, S.; Schönherr, H.; Vancso, G. J.; Kuipers, L. *J. Am. Chem. Soc.* **2004**, *126*, 1577–84.

(18) Beulen, M. W.; Bugler, J.; de Jong, M. R.; Lammerink, B.; Huskens, J.; Schönherr, H.; Vancso, G. J.; Boukamp, B. A.; Wieder, H.; Offenhauser, A.; Knoll, W.; van Veggel, F. C.; Reinhoudt, D. N. *Chem.-Eur. J.* **2000**, *6*, 1176–83.

(19) (a) Mulder, A.; Onclin, S.; Peter, M.; Hoogenboom, J. P.; Beijleveld, H.; ter Maat, J.; Garcia-Parajo, M. F.; Ravoo, B. J.; Huskens, J.; van Hulst, N. F.; Reinhoudt, D. N. *Small* **2005**, *1*, 242–53. (b) Thompson, D. *Langmuir* **2007**, *23*, 8441–51.

(20) Hinterdorfer, P.; Kienberger, F.; Raab, A.; Gruber, H. J.; Baumgartner, W.; Kada, G.; Riener, C.; Wielert-Badt, S.; Borken, C.; Schindler, H. *Single Mol.* **2000**, *1*, 99–103.

(21) Test fits of similar quality were obtained using the freely jointed chain (FJC) model. WLC was preferred due to its availability in the employed data analysis tool (Hooke, see ref 32).

(22) (a) Oesterhelt, F.; Rief, M.; Gaub, H. E. *New J. Phys.* **1999**, *1*, 1–11. (b) Thormann, E.; Hansen, P. L.; Simonsen, A. C.; Mouritsen, O. G. *Colloids Surf., B* **2006**, *53*, 149–56.

(23) Bell, G. I. *Science* **1978**, *200*, 618–627.

(24) Schönherr, H.; Beulen, M. W. J.; Bugler, J.; Huskens, J.; van Veggel, F. C. J. M.; Reinhoudt, D. N.; Vancso, G. J. *J. Am. Chem. Soc.* **2000**, *122*, 4963–4967.

(25) Zou, S.; Schönherr, H.; Vancso, G. J. *J. Am. Chem. Soc.* **2005**, *127*, 11230–1.

(26) Novo, M.; Granadero, D.; Bordello, J.; Al-Soufi, W. *J. Inclusion Phenom. Macrocyclic Chem.* **2010**, *11*, 173–188.

(27) Diezemann, G.; Janshoff, A. *J. Chem. Phys.* **2008**, *129*, 084904.

(28) (a) Seifert, U. *Phys. Rev. Lett.* **2000**, *84*, 2750–3. (b) Tees, D. F. J.; Woodward, J. T.; Hammer, D. A. *J. Chem. Phys.* **2001**, *114*, 7483–7496.

(29) Rao, J.; Lahiri, J.; Isaacs, L.; Weis, R. M.; Whitesides, G. M. *Science* **1998**, *280*, 708–11.

(30) Krishnamurthy, V. M.; Estroff, L. A.; Whitesides, G. M. *Multivalency in Ligand Design*; Wiley-VCH Verlag GmbH & Co. KGaA: New York, 2006; pp 11−53.

(31) The approximate value of k_{off} for a monovalent complex is deduced from the equilibrium constant in solution $K_{eq\text{-}M}$ (4.6×10^4 M^{-1}) and a diffusion-limited on-rate $k_{on} = 10^8$ M^{-1} s^{-1} (see refs 16a and 26).

(32) Sandal, M.; Benedetti, F.; Brucale, M.; Gomez-Casado, A.; Samori, B. *Bioinformatics* **2009**, *25*, 1428–30.

(33) RDC-Team, http://www.R-project.org, 2008.

(34) Sheather, S. J.; Jones, M. C. *J. R. Stat. Soc. B Met.* **1991**, 683–690.